Facile SILAR Approach to Air-Stable Naked Silver and Gold Nanoparticles Supported by Alumina

Kevin G. Stamplecoskie*[†,‡] and Joseph S. Manser[†,§]

[†]Radiation Laboratory, University of Notre Dame, Notre Dame, Indiana 46556, United States

[‡]Department of Chemistry and Biochemistry, University of Notre Dame, Notre Dame, Indiana 46556, United States

[§]Department of Chemical and Biomolecular Engineering, University of Notre Dame, Notre Dame, Indiana 46556, United States

Ⓢ *Supporting Information*

ABSTRACT: A synthetically convenient and scalable SILAR (successive ion layer adsorption and reaction) method is used to make air-stable films of silver and gold nanoparticles supported on alumina scaffolds. This solution-based deposition technique yields particles devoid of insulating capping agents or ligands. The optical properties of the nanoparticle films were investigated using femtosecond transient absorption spectroscopy. A linear absorption arising from intraband excitation (775 nm laser pulse) is seen only for Au nanoparticles at low intensity. However, both Au and Ag particles exhibit plasmon resonance responses at high excitation intensity via two photon absorption of the 775 nm pump pulse. The difference in optical response to near-IR laser excitation is rationalized based on the known density of states for each metal. To demonstrate the potential applications of these films, alumina-supported Ag nanoparticles were utilized as substrates for surface enhanced Raman spectroscopy, resulting in a 65-fold enhancement in the Raman signal of the probe molecule rhodamine 6G. The exceptional stability and scalability of these SILAR films opens the door for further optical and photocatalytic studies and applications, particularly with ligand-free Ag nanoparticles that typically oxidize under ambient conditions. Additionally, isolating plasmonic and interband electronic excitations in stable AgNP under visible light irradiation could enable elucidation of the mechanisms that drive noble metal-assisted photocatalytic processes.

KEYWORDS: metal nanoparticles, SILAR, metal oxide, femtosecond, ultrafast transient spectroscopy, two photon absorption
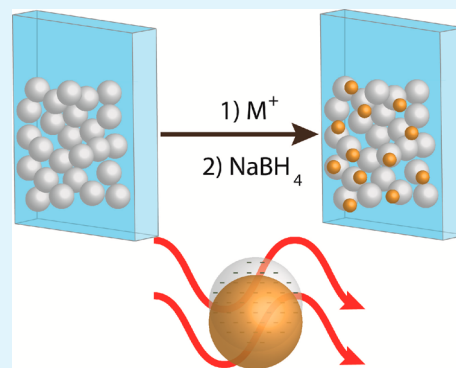
■ INTRODUCTION

Metal nanoparticles (NP) supported on metal oxides have become intensely investigated systems as a result of their interesting optical and catalytic properties.[1−12] Of particular interest is the research in catalysis and photocatalysis using gold nanoparticles (AuNP), which has seen a phenomenal increase following the realization that nanoscopic gold can be an active and selective air-stable catalyst.[13−21] Conversely, other metal nanoparticles, such as AgNP, have not received this same degree of attention, partly due to the instability of silver toward oxidation in air.[37] There have been a limited number of reports showing anomalous stabilization of AgNP in their metallic form on Al_2O_3 scaffolds for use in catalytic systems.[22−27] However, methods for preparing metal oxide-supported AgNP have thus far been limited to complicated laser-induced nanoparticle formation, vapor phase deposition and/or high temperature H_2 gas reduction of the adsorbed metal ions.[22−26]

Discussion of the role of short-lived excitation and excited state behavior of metal nanoparticles has been important for the development of optoelectronic and nanophotonic applications based on these materials.[2−4,20] The plasmon excitation and decay dynamics of AuNP have been extensively studied by pump−probe spectroscopic techniques such as femtosecond transient absorption spectroscopy.[5−7,12,28] For gold colloids, it has been shown that surface functionalization[29] and pump power/wavelength[5,7] can significantly influence the lifetime of the excited nanoparticle. There have, however, been few studies on the femtosecond excitation of AgNP, as detailed investigations are hampered by the inherent instability of these particles in solution and on most supports.[30−32]

Successive ion layer adsorption and reaction (SILAR) has become a common approach to synthesizing metal chalcogenide semiconductor quantum dots supported on metal oxides.[33−36] The approach, as the name suggests, involves submerging metal oxide substrates in an alternating fashion into solutions containing cation and anion precursors.[36] The absence of stabilizing ligands eliminates the need for long adsorption/chemisorption steps necessary for colloidal quantum dot deposition, and renders the particle surface free to interact chemically and electronically with the local environment.

Obviously, it is curious to explore whether a similar approach can be used to control the metal particle deposition on a mesoscopic metal oxide film. A SILAR-inspired method for the deposition of AuNP and AgNP on Al_2O_3 has been carried out with the aim to characterize the morphology and optical activity. It is important to note that unlike more arduous deposition methods previously reported, the SILAR approach for the formation of AgNP/AuNP provides air-stable nanoparticles by a simple, low-cost method that can easily be scaled to large wafers. Furthermore, the particles are free of surface functionalizing ligands, rendering them amenable to further investigating their interaction with ligands or other materials. The formation of metal nanoparticles on Al_2O_3 films, their characterization with scanning transmission electron microscopy (STEM) and X-ray diffraction (XRD), and their response to 775 nm laser pulse excitation are presented. Additionally, surface enhanced Raman spectroscopy (SERS) is used to demonstrate the effectiveness of these films in optical and catalytic applications.

■ EXPERIMENTAL SECTION

Film Fabrication. Glass microscope slides used as substrates for depositing metal oxide films were cleaned by ultrasonication in a detergent solution followed by rinsing with deionized water and ethanol and heating to 500 °C for 10 min to remove any residual organics. Films of Al_2O_3 were made by applying a paste containing 4.5 g of α-terpinol, 0.25 g of ethyl cellulose, 0.75 mL of benzyl alcohol and 0.4 g of Al_2O_3 (Degussa Aluminumoxid C, ~13 nm) with a doctor blade technique and drying at 80 °C for 30 min followed by annealing at 500 °C for 30 min. For deposition of noble metal nanoparticles, the Al_2O_3 films were dipped for 10 s in aqueous 10 mM metal salt ($AgNO_3$ or $HAuCl_4$), rinsed with water and dipped for 10 s in 10 mM $NaBH_4$ solution to reduce the metal. One such "cycle" of metal deposition is illustrated in Scheme 1, and the process was repeated for

higher loading. The method works equally well for doctor bladed films of TiO_2 (using Solaronix Ti Nanoxide T/SP) where AuNP deposition is higher than on Al_2O_3 (see Figure S1, Supporting Information). However, AgNP deposited on TiO_2 are not stable due to a well-documented visible light (room light) driven oxidation of AgNP on TiO_2.[38−40]

Characterization. Scanning transmission electron micrographs and energy dispersive X-ray spectra were obtained using an FEI Titan 80-300 TEM equipped with a high angle annular dark field detector and an Oxford INCA energy-dispersive X-ray spectroscopy (EDS) detector at an accelerating voltage of 300 keV. The metal particle-loaded metal oxide films were removed from the glass substrate and drop cast on copper grids for STEM and EDS measurements.

Optical absorbance spectra were recorded using a Cary 50, UV−vis spectrophotometer from Varian. Washed glass slides were used as a blank and scattering by Al_2O_3 alone is shown in absorbance spectra.

X-ray diffraction on Al_2O_3 and TiO_2 films was performed using a D8 ADVANCE DAVINCI powder XRD instrument from Bruker with a maximum resolution of 0.0001°. Samples were accumulated for several hours to improve signal-to-noise, especially due to the low overall quantities of nanoparticles deposited on the supports.

Ultrafast transient absorption techniques were performed using a Clark laser with a 775 nm fundamental pulsed at 1 kHz with 130 fs full-width at half maximum (fwhm) pulse durations. The fundamental is split to generate a white light probe by focusing through a Ti−saphire crystal. For 387 nm excitation, the second harmonic of the 775 nm is generated and used to excite samples. In this pump−probe setup, the transient absorption spectrum is recorded as a difference between probe signals with/without a pump pulse, and the delay between pump and probe is controlled to generate spectra at varied times following excitation.

Raman spectra were recorded with an NRS-5100 micro-Raman spectrometer from Jasco capable of detecting Raman shifts between 50−8000 cm^{-1}. The Raman spectrometer is equipped with 532 and 785 nm lasers for excitation and 5×, 20× and 100× magnification microscope. All samples were focused and recorded with the same integration time.

■ RESULTS AND DISCUSSION

Typically, a surface protector such as citric acid or a polymer is necessary to stabilize metal nanoparticles in aqueous or nonaqueous suspension. These metal nanoparticles are then deposited onto various substrates to carry out catalytic or sensing experiments. The SILAR method employed in this study offers a convenient method to load naked Ag and Au on alumina films with controlled particle density. During the first SILAR cycle, the seeds of metal nanoparticles are formed on the alumina surface as the metal ions are adsorbed and then reduced by BH_4^- ions. During the successive cycles, these seeds grow, ultimately reaching a densely covered metal particle film.

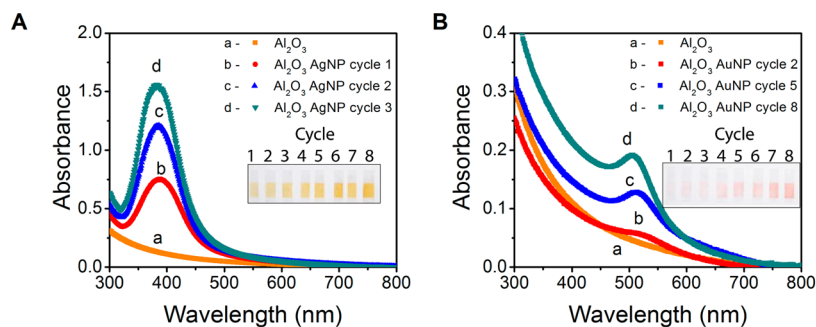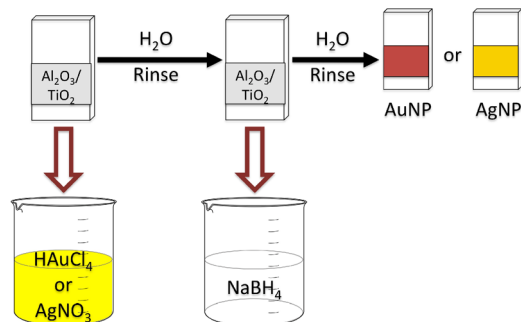**Scheme 1. Method for Making Stable Au/AgNP on Al_2O_3**

Figure 1. (A) Absorption spectra of AgNP deposited on Al_2O_3 films recorded after 1, 2 and 3 SILAR deposition cycles and (B) absorption spectra of AuNP deposited on Al_2O_3 films recorded after 2, 5 and 8 SILAR deposition cycles. Insets are images of Al_2O_3 films after 1−8 cycles of reaction as described in Scheme 1.
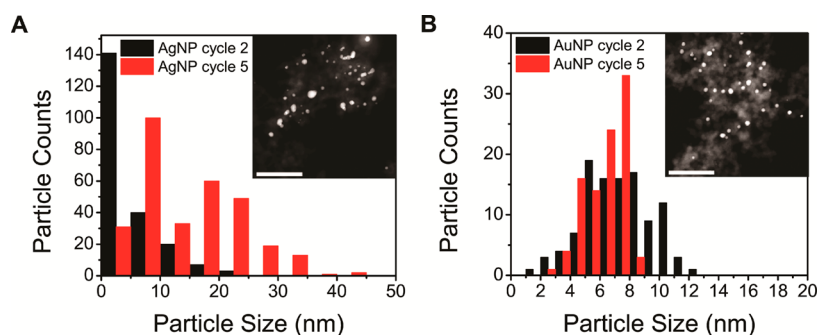
Figure 2. Histogram of nanoparticles sizes after 2 and 5 reaction cycles for (A) AgNP and (B) AuNP supported on Al_2O_3. The insets are representative STEM images of AgNP and AuNP on Al_2O_3 after 2 and 5 SILAR cycles, respectively. Scale bars are 100 nm.
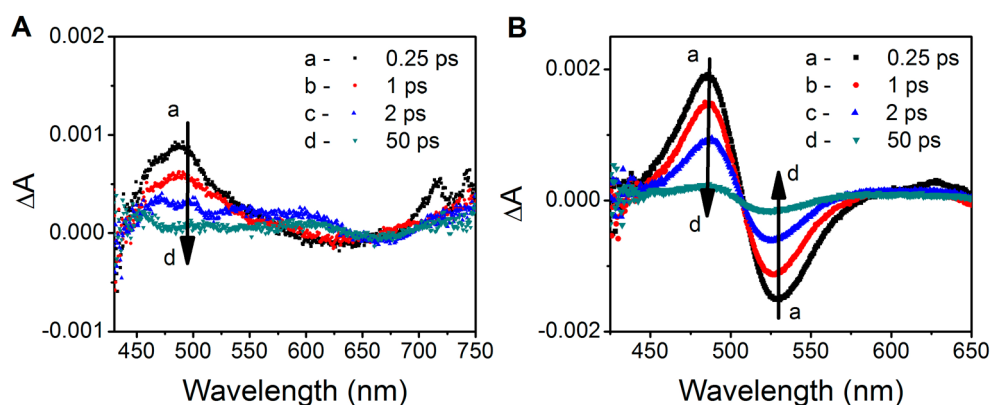

Figure 3. Transient absorption spectra of (A) AgNP and (B) AuNP on Al_2O_3 supports recorded at 0.25, 1, 2 and 50 ps after 775 nm excitation.

The loading of nanoparticles can be readily monitored by the absorption spectra after each SILAR cycle (Figure 1). The coloration of the Al_2O_3 film following the deposition of Ag and Au nanoparticles at successive cycles (inset in Figure 1) confirms the deposition of metal nanoparticles. It is evident from these images as well as the absorption spectra that the loading of AgNP onto Al_2O_3 saturates the absorption at only 3 SILAR cycles, whereas the loading and absorption of AuNP is markedly less even up to 8 SILAR cycles. Note that the maximum absorbance for AuNP films is ∼5 times smaller than that for the AgNP films. A Slower rate of adsorption of metal ions as well as differences in extinction are expected to contribute to the lower absorbance in AuNP loaded Al_2O_3 films. It should be noted that Ag^+ ions have a stronger affinity for the hydroxylated surface of Al_2O_3.[22]

The metal nanoparticles deposited on Al_2O_3 films were also characterized by XRD (see Figure S2, Supporting Information) and STEM (scanning transmission electron microscopy). The large z-contrast afforded by high angle annular dark field STEM enables effective resolution of small AgNP on Al_2O_3. Energy dispersive X-ray spectroscopic mapping in Figure S3 (Supporting Information) demonstrates the significant contrast between AgNP and the metal oxide support. Particle size histograms were generated from STEM images with samples of 2 and 5 SILAR cycles. It is clear from the histogram in Figure 2A that the AgNP size has a large polydispersity and that the size distribution increases with increasing reaction cycles (mean diameter = 5.5 ± 4.3 nm after 2 reaction cycles and 14.1 ± 9.0 nm after 5 cycles). AuNP on Al_2O_3, however, have a narrower size distribution that does not change significantly with increased number of cycles, with very few of the particles

below 4 nm in diameter (mean diameter = 7.3 ± 2.2 nm after 2 reaction cycles and 6.2 ± 1.3 nm after 5 cycles).

It is interesting to note that the nanoparticles deposited on Al_2O_3 are well dispersed. This observation is consistent with plasmon absorption in Figure 1 that is similar to well dispersed Au/AgNP colloids. The narrow plasmon band and lack of absorption to the red of the plasmon resonance indicate minimal aggregation and absence of anisotropic particles on Al_2O_3 supports.[40,41]

Femtosecond transient absorption spectroscopy serves as a convenient tool for characterization of metal nanoparticles. These nanoparticles can be excited with energy greater than the plasmon resonance (387 nm femtosecond laser pulse excitation) and induce bleaching of the plasmon resonance. This monophotonic process can be induced using a relatively low power excitation pulse. The representative transient spectra recorded with 387 nm laser pulse excitation are shown in Figure S4 (Supporting Information). The bleaching recovery in these experiments corresponds to electron−phonon and phonon−medium interactions,[6,12] as discussed below.

In the present study, we employ two photon excitation to elucidate the ultrafast photodynamics of Au and AgNP deposited on Al_2O_3 films. A thorough understanding of the excitation and relaxation dynamics of the alumina-supported metal particles is vital for optimization of optical and photocatalytic systems employing these SILAR films. Transient absorption spectra were recorded at various delay times after 775 nm laser pulse excitation (energy 40 mW/cm^2, 130 fs fwhm and a 1 kHz repetition rate) of the metal particles anchored on Al_2O_3 films. The transient absorption spectra recorded with AgNP and AuNP deposited on Al_2O_3 films are shown in Figure 3A,B, respectively.

It is interesting that upon excitation with a 775 nm (two photon) pump pulse, the metal nanoparticles exhibit a transient response similar to that observed with 387 nm (single photon). The transient spectra obtained with $AuNP/Al_2O_3$ exhibit a bleaching at 532 nm and an induced absorption maximum at 480 nm. These spectral changes are attributed to dampening of the surface plasmon band. For $AgNP/Al_2O_3$ films, we observe only an induced absorption at 500 nm. Because of the limitations of detection wavelength in the current experimental setup, we were not able to probe the bleaching of the surface plasmon absorption.

The lifetime of the decay of the AgNP under laser excitation could be fit to biexponential decay kinetics, with a fast component of 1.5 ± 0.1 ps and a long component of 75 ± 43 ps (see Figure S5, Supporting Information). The AuNP transient signal at 530 nm was also fit using a biexponential expression and exhibits a short lifetime of 2.65 ± 0.03 ps and a long lifetime component of 223 ± 19 ps. The lifetimes for the ΔA signal of both nanoparticles are summarized in Table S1 (Supporting Information). These transient decay lifetimes are typical for noble metal nanoparticles that are subjected to surface plasmon excitation. There are four main processes involved in relaxation after plasmon excitation: (i) electron dephasing ($\sim$10 fs), (ii) electron−electron scattering ($\sim$100 fs), (iii) electron−phonon scattering ($\sim$1 ps) and (iv) phonon−phonon relaxation or transfer of energy to the surroundings (hundreds of picoseconds). Only the latter two processes can be time-resolved in the experiments herein. The fast component of the decay that we observe corresponds to electron−phonon interactions due to collisions of oscillating electrons with nuclei. The long component arises as a result of slower phonon−phonon interactions that transfer heat from the particle to the surroundings.[6,12] The short lifetime of the decay is known to be a function of excitation power, but the particle size does not significantly impact this decay component.[6,29]

The maximum $|\Delta A|$ as a function of laser power can be used to determine whether the excitation is a single or multiphoton process. The data can be fit to the following function:

$$\Delta A = C \times (\text{laser power})^B \quad (1)$$

where C is a constant and B indicates the order of the process. It is common practice use the linear slope of a log−log plot of absorbed photons (or emission counts for emissive species) versus laser power to determine the order of the excitation mechanism.[42,43] The maximum ΔA at 500 nm upon excitation of AgNP on Al_2O_3 is plotted in Figure 4A as a function of 775 nm pump power. Similarly, the maximum bleach in absorbance for AuNP at 530 nm is plotted in Figure 4B as a function of laser power. Note that the bleach maximum for AgNP ($\sim$400 nm) is outside the probe wavelength range ($>$430 nm), hence we could employ only the induced absorption for monitoring the power dependence. For AuNP, however, both the maximum bleach at 530 nm and the maximum positive ΔA at 480 nm can be monitored versus laser power. These two monitoring wavelengths give identical dependence on the incident laser power (see Figure S6, Supporting Information).

Two noticeable trends are evident in Figure 4A: (i) a clear threshold at 15 mW/cm^2, below which there is no observable excitation response from AgNP and (ii) a linear dependence of the excitation versus laser power above this threshold (see Figure S7, Supporting Information for kinetic traces above and below the two photon excitation threshold of AgNP). When
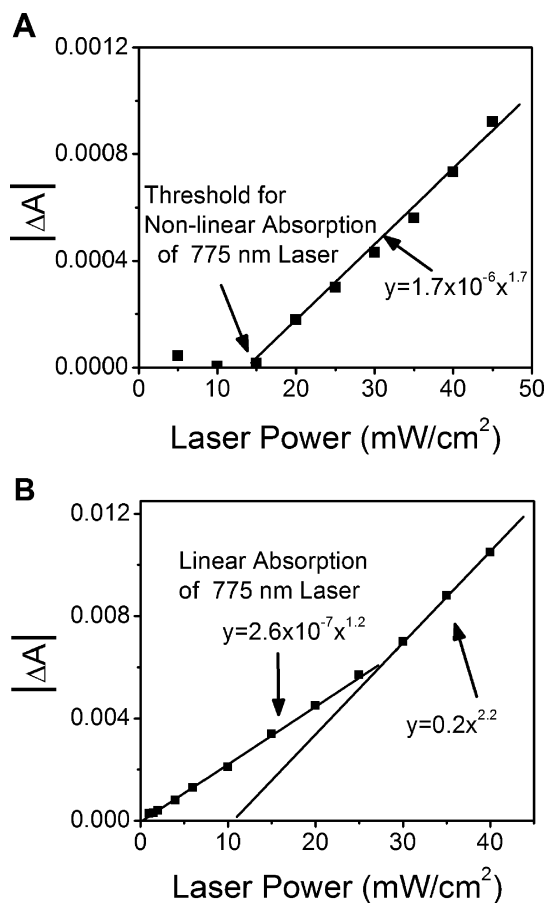

Figure 4. (A) Maximum $|\Delta A|$ at 500 nm for AgNP on Al_2O_3 and (B) maximum $|\Delta A|$ at 530 nm for AuNP on Al_2O_3 as a function of 775 nm laser power. Linear fits to eq 1 are shown for the different linear regions as indicated.

the $|\Delta A|$ above 15 mW/cm^2 is fit to eq 1, a value of 1.7 is found for B, which can be approximated as 2. Both the observation of an excitation threshold and slope of $\sim$2 indicates that the excitation of AgNP occurs exclusively through a two photon process, and that there is no linear excitation of these particles. Though power dependence for two photon excitation is commonly presented in log−log plots, the threshold for two photon excitation is more difficult to visualize here. The data in Figure 4A,B is shown on a double-log plot in Figure S8 (Supporting Information). From the log−log plots, it is also clear that there is only one linear region for AgNP that represents two photon excitation, whereas AuNP display both one and two photon response.

The dependence of $|\Delta A|$ on excitation power for AuNP on Al_2O_3 in Figure 4B shows a very different response from that of AgNP. There is no distinct threshold for excitation, and instead we observe two distinct linear regions that, when fit to eq 1, have B values of 1.2 ($\sim$1) and 2.2 ($\sim$2). This result indicates that AuNP demonstrate linear absorption of 775 nm light along with significant two photon absorption above a laser power of approximately 30 mW/cm^2.

The different susceptibility of AgNP and AuNP can be understood from the band structure and absorption spectra for colloids of each of these nanoparticles. Representative absorption spectrum of citrate stabilized AgNP and AuNP are provided in Figure 5, as well as an illustration of the corresponding density of states for each metal. The absorption
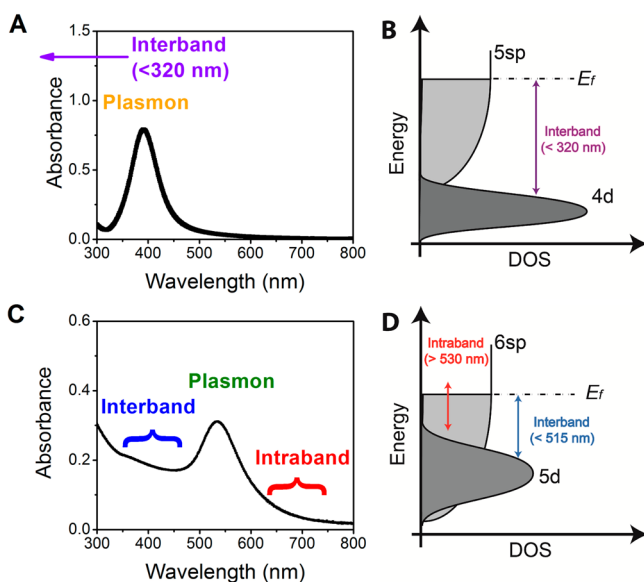
Figure 5. Absorption spectra of citrate stabilized (A) AgNP and (C) AuNP and corresponding density of states diagrams for each metal in panels B and D, respectively.
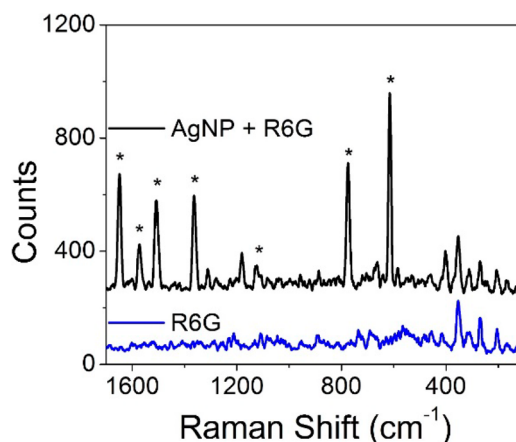

Figure 6. Raman spectrum of rhodamine 6G dried on an Al_2O_3 film (R6G) and SERS spectrum of rhodamine 6G dried on an AgNP/Al_2O_3 film (AgNP + R6G). The peaks labeled with an asterisk have been assigned to vibrational modes of rhodamine 6G.[45]

spectrum for AgNP only includes a plasmon absorption centered at approximately 400 nm for spherical colloids. The onset of interband transitions for AgNP does not occur until below 320 nm.[12,44] Therefore, the two photon absorption of AgNP on Al_2O_3 is simply a two photon excitation of the plasmon absorption.

The absorbance spectrum of spherical AuNP, however, is complicated due to the overlap of plasmon absorption, centered at 530 nm, with interband/intraband transitions.[12] The excitation of AuNP with 775 nm femtosecond laser pulses below the two photon threshold is a direct excitation of intraband transitions, with a small probability of direct plasmon or interband excitation. The two photon absorption that occurs at higher laser powers is a result of interband transitions that rapidly decay into a hot plasmon.[12,44]

This SILAR approach for fabrication of Al_2O_3 supported AgNP and AuNP can be a convenient way to make solid supported and stable nanoparticle substrates for studies in a variety of different applications. We have performed surface enhanced Raman spectroscopy (SERS) measurements to illustrate the activity of the nanoparticles, specifically AgNP, in enhancing the Raman spectrum of a common SERS probe, rhodamine 6G. In these experiments, one drop of 1 mM rhodamine 6G dissolved in ethanol was allowed to dry on each of the substrates. The Raman spectra were acquired using a 532 nm continuous wave laser. The peaks in the Raman spectra shown in Figure 6 match those of R6G previously reported (613, 775, 1130, 1364, 1512, 1577 and 1651 cm^{-1}).[45,46] The enhancement factor (G) was calculated using eq 2 and the intensity of the characteristic 1364 cm^{-1} Raman peak (~650 counts with AgNP and ~10 counts for R6G alone, without any nanoparticles). In both cases, the same amount of rhodamine 6G was dried on the substrate, so the concentration (M) is equal for measurements with and without nanoparticles.

$$G = \frac{I_{SERS}}{I_{Raman}} \times \frac{M_{Raman}}{M_{SERS}} \quad\quad (2)$$

According to eq 2, the AgNP substrate gives a SERS enhancement factor of ~65 for R6G.

The SERS measurements are performed here to illustrate one possible application of the AgNP made by this simple SILAR method. There are a number of SERS studies using AgNP that find enhancement factors with reported values as high as 10^7–10^{14}.[46,53−55] The enhancement factor, for example, is known to be dependent on nanoparticle size, due in part to the increasing field enhancement for larger particles as well as increased scattering efficiency.[46] The AgNP made here have a polydispersity (14.1 ± 9.0 nm), which can result in a nonhomogeneous SERS enhancement over the substrate surface on the nanometer scale, where larger particles contribute more to the SERS signal. The largest reported enhancement factors in SERS are for areas of high field enhancement between aggregates of particles.[53] As discussed above, STEM images reveal minimal aggregation of AgNP across the alumina surface. This may in part explain the relatively low enhancement factor obtained here. Similar to the variation due to size distribution, the absolute intensity of the SERS signal may vary on the nanoscale here due to aggregate hot spots, but these areas are randomly distributed over the substrate. The spatial resolution of the SERS measurements here is not sufficient to investigate the individual SERS intensity of particles on the substrate. However, different regions of the substrate gave similar SERS enhancement, indicating a uniform SERS enhancement at least on the macroscopic scale.

■ CONCLUSION

A solution-based dip or SILAR method for making stable films of AgNP and AuNP supported on mesoscopic Al_2O_3 with tunable particle loading is presented. This synthetically simple preparation method yields metal oxide films decorated with metal nanoparticles that exhibit significant surface plasmon activity. The 775 nm excitation of AgNP is purely a two photon process, whereas AuNP respond to both linear (low power) and two photon (high power) excitations. To illustrate potential applications of these films, stable AgNP on Al_2O_3 were shown to exhibit SERS activity in the enhancement of rhodamine 6G.

The particles made by this method have no additional stabilizing agents, leaving their surfaces exposed for adsorption

of desired ligands or probe molecules. These films can be submerged in solutions to adsorb analytes or can be coated with desired materials. Although the polydispersity of the SILAR films has little effect on the excited state lifetimes of the embedded NPs, in certain photocatalytic and sensing systems, variability in size has been shown to impact the performance of metal−semiconductor and metal−adsorbate nanocomposite materials.[47] Moving forward, better control over the size distribution of metal NPs in these metal oxide scaffolds would enable facile fabrication of functional films with tailored optical and electronic properties.

Furthermore, the mechanism by which these nanoparticles are active in photocatalysis, particularly AuNP, is a highly deliberated subject. The question arises whether photocatalysis using AuNP relies on electron transfer, plasmon enhancement of electronic transitions, or simply photothermal effects that occur upon excitation of the particles.[20,48−52] In the case of AgNP, it is possible to isolate plasmonic effects from direct interband transitions within the visible spectrum. Therefore, disparities in the photocatalytic activity of supported AgNP and AuNP can be used to obtain insight into the mechanisms that drive such processes in metal nanoparticle systems.

■ ASSOCIATED CONTENT

Ⓢ Supporting Information

(S1) Loading of Au and AgNP on mesoporous TiO_2 scaffolds demonstrating the inherent oxidation of AgNP supported on titania. (S2) XRD patterns of Au and AgNP on Al_2O_3 and TiO_2. (S3) STEM EDX mapping of AgNP on Al_2O_3. (S4) Representative transient absorption spectra demonstrating monophotonic absorption in both Au and AgNP following 387 nm laser pulse excitation. (S5) Transient kinetic of Au and AgNP on Al_2O_3 after 775 nm excitation. (Table S1) Summary of excited state lifetimes. (S6) Power dependence of the maximum $|\Delta A|$ at 480 and 530 nm for AuNP on Al_2O_3. (S7) Transient absorption time-decay profiles for AgNP on Al_2O_3 monitored at 500 nm. (S8) Log−log plots of the plasmon excitation for AgNP (A) and AuNP (B) as a function of laser power. This material is available free of charge via the Internet at http://pubs.acs.org.

■ AUTHOR INFORMATION

Corresponding Author
*K. G. Stamplecoskie. E-mail: kstample@nd.edu.

Notes
The authors declare no competing financial interest.

■ ACKNOWLEDGMENTS

■ REFERENCES

(1) Eustis, S.; El-Sayed, M. A. Why Gold Nanoparticles Are More Precious than Pretty Gold: Noble Metal Surface Plasmon Resonance and Its Enhancement of the Radiative and Nonradiative Properties of Nanocrystals of Different Shapes. *Chem. Soc. Rev.* **2006**, *35*, 209−217.

(2) Berini, P.; De Leon, I. Surface Plasmon−Polariton Amplifiers and Lasers. *Nat. Photonics* **2011**, *6*, 16−24.

(3) Noginov, M. A.; Zhu, G.; Belgrave, A. M.; Bakker, R.; Shalaev, V. M.; Narimanov, E. E.; Stout, S.; Herz, E.; Suteewong, T.; Wiesner, U. Demonstration of a Spaser-based Nanolaser. *Nature* **2009**, *460*, 1110−1112.

(4) Stockman, M. I. The Spaser as a Nanoscale Quantum Generator and Ultrafast Amplifier. *J. Opt.* **2010**, *12*, 24004.

(5) Smith, B. A.; Zhang, J. Z.; Giebel, U.; Schmid, G. Direct Probe of Size-Dependent Electronic Relaxation in Single-Sized Au and Nearly Monodisperse Pt Colloidal Nano-Particles. *Chem. Phys. Lett.* **1997**, *270*, 139−144.

(6) Link, S.; Burda, C.; Wang, Z. L.; El-Sayeda, M. A. Electron Dynamics in Gold and Gold−Silver Alloy Nanoparticles: The Influence of a Nonequilibrium Electron Distribution and the Size Dependence of the Electron−Phonon Relaxation. *J. Chem. Phys.* **1999**, *111*, 1255−1264.

(7) Mohamed, M. B.; Ahmadi, T. S.; Link, S.; Braun, M.; El-Sayed, M. A. Hot Electron and Phonon Dynamics of Gold Nanoparticles Embedded in a Gel Matrix. *Chem. Phys. Lett.* **2001**, *343*, 55−63.

(8) Sivapalan, S. T.; Vella, J. H.; Yang, T. K.; Dalton, M. J.; Swiger, R. N.; Haley, J. E.; Cooper, T. M.; Urbas, A. M.; Tan, L. S.; Murphy, C. J. Plasmonic Enhancement of the Two Photon Absorption Cross Section of an Organic Chromophore Using Polyelectrolyte-Coated Gold Nanorods. *Langmuir* **2012**, *28*, 9147−9154.

(9) Kelly, K. L.; Coronado, E.; Zhao, L. L.; Schatz, G. C. The Optical Properties of Metal Nanoparticles: The Influence of Size, Shape, and Dielectric Environment. *J. Phys. Chem. B* **2003**, *107*, 668−677.

(10) Coronado, E. A.; Encina, E. R.; Stefani, F. D. Optical Properties of Metallic Nanoparticles: Manipulating Light, Heat and Forces at the Nanoscale. *Nanoscale* **2011**, *3*, 4042−4059.

(11) Slaughter, L.; Chang, W. S.; Link, S. Characterizing Plasmons in Nanoparticles and Their Assemblies with Single Particle Spectroscopy. *J. Phys. Chem. Lett.* **2011**, *2*, 2015−2023.

(12) Hartland, G. V. Optical Studies of Dynamics in Noble Metal Nanostructures. *Chem. Rev.* **2011**, *111*, 3858−3887.

(13) Haruta, M. Size- and Support-Dependency in the Catalysis of Gold. *Catal. Today* **1997**, *36*, 153−166.

(14) Hayashi, T.; Tanaka, K.; Haruta, M. Selective Vapor-Phase Epoxidation of Propylene over Au/TiO_2 Catalysts in the Presence of Oxygen and Hydrogen. *J. Catal.* **1998**, *178*, 566−575.

(15) Yan, J. M.; Zhang, X. B.; Akita, T.; Haruta, M.; Xu, Q. One-Step Seeding Growth of Magnetically Recyclable Au@Co Core-Shell Nanoparticles: Highly Efficient Catalyst for Hydrolytic Dehydrogenation of Ammonia Borane. *J. Am. Chem. Soc.* **2010**, *132*, 5326−5327.

(16) Corma, A.; Juárez, R.; Boronat, M.; Sánchez, F.; Iglesias, M.; García, H. Gold Catalyzes the Sonogashira Coupling Reaction without the Requirement of Palladium Impurities. *Chem. Commun.* **2011**, *47*, 1446−1448.

(17) Corti, C.; Holliday, R.; Thompson, D. Progress towards the Commercial Application of Gold Catalysts. *Top. Catal.* **2007**, *44*, 331−343.

(18) Heck, K.; Nutt, M.; Alvarez, P.; Wong, M. Deactivation Resistance of Pd/Au Nanoparticle Catalysts for Water-Phase Hydrodechlorination. *J. Catal.* **2009**, *267*, 97−104.

(19) Hutchings, G. Nanocrystalline Gold and Gold−Palladium Alloy Oxidation Catalysts: A Personal Reflection on the Nature of the Active Sites. *Dalton Trans.* **2008**, 5523−5536.

(20) Primo, A.; Corma, A.; García, H. Titania Supported Gold Nanoparticles as Photocatalyst. *Phys. Chem. Chem. Phys.* **2011**, *13*, 886−910.

(21) Haruta, M.; Kobayashi, T.; Sano, H.; Yamada, N. Novel Gold Catlysis for the Oxidation of Carbon Monoxide at a Temperature Far Below 0C. *Chem. Lett.* **1987**, *16*, 405−408.

(22) Esteban-Cubillo, A.; Díaz, C.; Fernández, A.; Díaz, L.; Pecharromán, C.; Torrecillas, R.; Moya, J. Silver Nanoparticles Supported on A-, H- and Δ-Alumina. *J. Eur. Cer. Soc.* **2006**, *26*, 1−7.

(23) Huang, W. X.; Teng, J.; Cai, T.; Bao, X. Silver as a Promoter for the Catalytic Decomposition of NO_x under Oxygen-Excess Condition:

Evidence for Oxygen Spillover from Noble Metals to Silver. *Stud. Surf. Sci. Catal.* **2000**, *130*, 1409.

(24) Miyadera, T. Alumina-Supported Silver Catalysts for the Selective Reduction of Nitric Oxide with Propene and Oxygen-Containing Organic Compounds. *Appl. Catal., B* **1993**, *2*, 199−205.

(25) Miyadera, T. Selective Reduction of Nitric Oxide with Ethanol over an Alumina-Supported Silver Catalyst. *Appl. Catal., B* **1997**, *13*, 157−165.

(26) Miyadera, T. Selective Reduction of NO_x by Ethanol on Catalysts Composed of Ag/Al_2O_3 and Cu/TiO_2 without Formation of Harmful by-Products. *Appl. Catal., B* **1998**, *16*, 155−164.

(27) Poreddy, R.; García-Suárez, E. J.; Riisager, A.; Kegnæs, S. Silver Nanoparticles Supported on Alumina—A Highly Efficient and Selective Nanocatalyst for Imine Reduction. *Dalton Trans.* **2014**, *43*, 4255−4259.

(28) Link, S.; El-Sayed, M.; Schaaff, T.; Whetten, R. Transition from Nanoparticle to Molecular Behaviour: A Femtosecond Transient Absorption Study of a Size Selected 28 Atom Gold Cluster. *Chem. Phys. Lett.* **2002**, *356*, 240−246.

(29) Aruda, K.; Tagliazucchi, M.; Sweeney, C.; Hannah, D.; Schatz, G.; Weiss, E. Identification of Parameters through Which Surface Chemistry Determines the Lifetimes of Hot Electrons in Small Au Nanoparticles. *Proc. Natl. Acad. Sci. U. S. A.* **2013**, *110*, 4212−4217.

(30) Baraldi, G.; Carrada, M.; Toudert, J.; Ferrer, F. J.; Arbouet, A.; Paillard, V.; Gonzalo, J. Preventing the Degradation of Ag Nanoparticles Using an Ultrathin α-Al_2O_3 Layer as Protective Barrier. *J. Phys. Chem. C* **2013**, *117*, 9432−9439.

(31) Licea-Rodríguez, J.; Rocha-Mendoza, I.; Rangel-Rojo, R.; Rodríguez-Fernández, L.; Oliver, A. Femtosecond Laser Writing over Silver Nanoparticles System Embedded in Silica Using Nonlinear Microscopy. *Opt. Mater. (Amsterdam, Neth.)* **2014**, *36*, 682−686.

(32) Sung, J.; Kosuda, K. M.; Zhao, J.; Elam, J. W.; Spears, K. G.; Duyne, R. P. V. Stability of Silver Nanoparticles Fabricated by Nanosphere Lithography and Atomic Layer Deposition to Femtosecond Laser Excitation. *J. Phys. Chem. C* **2008**, *112*, 5707−5714.

(33) Jin, H.; Choi, S.; Lee, H. J.; Kim, S. Layer-by-Layer Assemblies of Semiconductor Quantum Dots for Nanostructured Photovoltaic Devices. *J. Phys. Chem. Lett.* **2013**, *4*, 2461−2470.

(34) Kamat, P. V. Boosting the Efficiency of Quantum Dot Sensitized Solar Cells through Modulation of Interfacial Charge Transfer. *Acc. Chem. Res.* **2012**, *45*, 1906−1915.

(35) Lee, H.; Leventis, H.; Moon, S.; Chen, P.; Ito, S.; Haque, S.; Torres, T.; Nüesch, F.; Geiger, T.; Zakeeruddin, S.; Grätzel, M.; Nazeeruddin, M. K. PbS and CdS Quantum Dot-Sensitized Solid-State Solar Cells: "Old Concepts, New Results". *Adv. Funct. Mater.* **2009**, *19*, 2735−2742.

(36) Santra, P. K.; Nair, P. V.; Thomas, K. G.; Kamat, P. V. $CuInS_2$-Sensitized Quantum Dot Solar Cell. Electrophoretic Deposition, Excited-State Dynamics, and Photovoltaic Performance. *J. Phys. Chem. Lett.* **2013**, *4*, 722−729.

(37) Naoi, K.; Ohko, Y.; Tatsuma, T. TiO_2 Films Loaded with Silver Nanoparticles: Control of Multicolor Photochromic Behavior. *J. Am. Chem. Soc.* **2004**, *126*, 3664−3668.

(38) Ohko, Y.; Tatsuma, T.; Fujii, T.; Naoi, K.; Niwa, C.; Kubota, Y.; Fujishima, A. Multicolour Photochromism of TiO_2 Films Loaded with Silver Nanoparticles. *Nat. Mater.* **2003**, *2*, 29−31.

(39) Rahbarpour, S.; Hosseini-Golgoo, S. M. Schottky Type $Ag-TiO_2$ Hydrogen Sensor: Gas Sensing Mechanism and Modeling. In *14th International Meeting on Chemical Sensors - IMCS 2012*, Nürnberg, Germany, May 20−23, 2012; AMA Service GmbH: Wunstorf, Germany, 2012; pp 1275−1278.

(40) Link, S.; Wang, Z. L.; El-Sayed, M. A. Alloy Formation of Gold-Silver Nanoparticles and the Dependence of the Plasmon Absorption on Their Composition. *J. Phys. Chem. B* **1999**, *103*, 3529−3533.

(41) Quinten, M. The Color of Finely Dispersed Nanoparticles. *Appl. Phys. B: Lasers Opt.* **2001**, *73*, 317−326.

(42) Guan, Z.; Gao, N.; Jiang, X.; Yuan, P.; Han, F.; Xu, Q. Huge Enhancement in Two-Photon Photoluminescence of Au Nanoparticle

Clusters Revealed by Single-Particle Spectroscopy. *J. Am. Chem. Soc.* **2013**, *135*, 7272−7277.

(43) Jiang, X.; Pan, Y.; Jian, C.; Zhao, T.; Yuan, P.; Venkatesan, T.; Xu, Q. Excitation Nature of Two-Photon Photoluminescence of Gold Nanorods and Coupled Gold Nanoparticles Studied by Two-Pulse Emission Modulation. *J. Phys. Chem. Lett.* **2013**, *4*, 1634−1638.

(44) Henglein, A. Physichochemical Properties of Small Metal Particles in Solution: "Microelectrode" Reactions, Chemisorption, Composite Metal Particles, and the Atom-to-Metal Transition. *J. Phys. Chem.* **1993**, *97*, 5457−5471.

(45) Watanabe, H.; Hayazawa, N.; Inouye, Y.; Kawata, S. DFT Vibrational Calculations of Rhodamine 6G Adsorbed on Silver: Analysis of Tip-Enhanced Raman Spectroscopy. *J. Phys. Chem. B* **2005**, *109*, 5012−5020.

(46) Stamplecoskie, K. G.; Scaiano, J. C.; Tiwari, V. S.; Anis, H. Optimal Size of Silver Nanoparticles for Surface-Enhanced Raman Spectroscopy. *J. Phys. Chem. C* **2011**, *115*, 1403−1409.

(47) Subramanian, V.; Wolf, E. E.; Kamat, P. V. Catalysis with TiO_2/ Gold Nanocomposites. Effect of Metal Particle Size on the Fermi Level Equilibration. *J. Am. Chem. Soc.* **2004**, *126*, 4943−4950.

(48) Silva, C. G.; Juárez, R.; Marino, T.; Molinari, R.; García, H. Influence of Excitation Wavelength (UV or Visible Light) on the Photocatalytic Activity of Titania Containing Gold Nanoparticles for the Generation of Hydrogen or Oxygen from Water. *J. Am. Chem. Soc.* **2011**, *133*, 595−602.

(49) Scaiano, J. C.; Stamplecoskie, K. Can Surface Plasmon Fields Provide a New Way to Photosensitize Organic Photoreactions? From Designer Nanoparticles to Custom Applications. *J. Phys. Chem. Lett.* **2013**, *4*, 1177−1187.

(50) Ha, J. W.; Ruberu, T. P. A.; Han, R.; Dong, B.; Vela, J.; Fang, N. Super-Resolution Mapping of Photogenerated Electron and Hole Separation in Single Metal-Semiconductor Nanocatalysts. *J. Am. Chem. Soc.* **2014**, *136*, 1398−1408.

(51) Hoggard, A.; Wang, L.; Ma, L.; Fang, Y.; You, G.; Olson, J.; Liu, Z.; Chang, W.; Ajayan, P. M.; Link, S. Using the Plasmon Linewidth To Calculate the Time and Efficiency of Electron Transfer between Gold Nanorods and Graphene. *ACS Nano* **2013**, *7*, 11209−11217.

(52) Kale, M. J.; Avanesian, T.; Christopher, P. Direct Photocatalysis by Plasmonic Nanostructures. *ACS Catal.* **2014**, *4*, 116−128.

(53) Mirsaleh-Kohan, N.; Iberi, V.; Simmons, P. D., Jr.; Bigelow, N. W.; Vaschillo, A.; Rowland, M. M.; Best, M. D.; Pennycook, S. J.; Masiello, D. J.; Guiton, B. S.; Camden, J. P. Single-Molecule Surface-Enhanced Raman Scattering: Can STEM/EELS Image Electromagnetic Hot Spots? *J. Phys. Chem. Lett.* **2012**, *3*, 2303−2309.

(54) Etchegoin, P. G.; Le Ru, E. C. A Perspective on single molecule SERS: Current Status and Future Challenges. *Phys. Chem. Chem. Phys.* **2008**, *10*, 6069−6200.

(55) Dieringer, J. A.; Lettan, R. B., II; Scheidt, K. A.; Van Duyne, R. P. A Frequency Domain Existence Proof of Single Molecule Surface-Enhanced Raman Spectroscopy. *J. Am. Chem. Soc.* **2007**, *129*, 16249−16256.